Engineering 15 (2022) 154–164

Contents lists available at ScienceDirect

Engineering

journal homepage: www.elsevier.com/locate/eng

Research
Environmental Engineering—Article

Unraveling Membrane Fouling Induced by Chlorinated Water Versus Surface Water: Biofouling Properties and Microbiological Investigation

Li Zhang [a,b], Lei Xu [a,*], Nigel Graham [c], Wenzheng Yu [a,*]

[a] State Key Laboratory of Environmental Aquatic Chemistry, Research Center for Eco-Environmental Sciences, Chinese Academy of Sciences, Beijing 100085, China
[b] University of Chinese Academy of Sciences, Beijing 100049, China
[c] Department of Civil and Environmental Engineering, Imperial College London, South Kensington Campus, London SW7 2AZ, UK

ARTICLE INFO

Article history:
Received 13 October 2020
Revised 1 December 2020
Accepted 5 March 2021
Available online 6 May 2021

Keywords:
Membrane fouling
Biofilm
GDM filtration technology
Ultrafiltration
Chlorine-resistant bacteria
Hydrophilicity

ABSTRACT

Chlorine is usually applied in the urban water treatment process to deactivate pathogens and prevent waterborne diseases. As a pre-treatment, it remains unclear whether chlorinated water can effectively alleviate membrane fouling during ultrafiltration (UF). In this study, tap water was investigated for its effect on biofilm formation and biofouling in a gravity-driven membrane (GDM) filtration system. For comparison, biofilm/biofouling with untreated surface (lake) water was studied in parallel. It was found that more severe membrane fouling occurred with the filtration of tap water than lake water, and larger quantities of polysaccharide and extracellular DNA (eDNA) were present in the tap-water biofilm than in the lake-water biofilm. The tap-water biofilm had a densely compact morphology. In contrast, a porous, spider-like structure was observed for the lake-water biofilm, which was assumed to be associated with the bacteria in the biofilm. This hypothesis was verified by 16S ribosomal RNA (rRNA) sequencing, which demonstrated that *Xanthobacter* was the dominant taxon in the tap-water biofilm. Additionally, membrane hydrophobicity/hydrophilicity played a minor role in affecting the membrane fouling properties and microbial community. This study revealed the significant role of chlorine-resistant bacteria in biofouling formation and provides a deeper understanding of membrane fouling, which can potentially aid in searching for effective ways of controlling membrane fouling.

1. Introduction

The availability of safe and plentiful drinking water is becoming increasingly limited worldwide, particularly in remote areas of developing countries [1]. Remote distances, scattered communities, and poor transport infrastructure make it difficult to provide and sustain adequate safe water supplies. Surface waters, including rivers and lakes, are less polluted in these remote areas; therefore, they can be used as sources for drinking water with a less-intensive treatment method. Membrane filtration technology, particularly ultrafiltration (UF) membrane technology [2], is an established and versatile method for water purification and drinking water production [3]. UF membranes can intercept suspended solids, colloids, and bacteria by size exclusion, as the pore diameter (approximately 100 kDa) is smaller than the size of these typical contaminants [4]. In addition, water can pass through UF membranes with a low transmembrane pressure, which can be achieved by a gravity-driven arrangement [5,6].

Gravity-driven membrane (GDM) filtration technology has gained attention and application in treating greywater [7,8], wastewater [9], rainwater [10], and pretreatment of seawater [11] owing to its extremely low energy consumption, no backwashing, and steady flux. The accumulated biofilm plays an essential role in the regulation of the GDM filtration system. First, the permeable biofouling layer acts as a secondary membrane [6] and maintains flux stability [5]. Second, it degrades organic substances [8,12]. Studies regarding critically important biofouling layer have varied from those related to the key parameters (e.g., feed water [5], aeration shear stress [13], biological control [14], and nutrient limiting [15]) to the links between biofilm morphology and filtration performance [2], aiming to reveal the properties of biofilms and, thus, effectively control their accumulation. In the effects of feed water, the concentration of dissolved organic matter (DOC) plays an important role and is negatively correlated with the

* Corresponding authors.
E-mail addresses: leixu@rcees.ac.cn (L. Xu), wzyu@rcees.ac.cn (W. Yu).

https://doi.org/10.1016/j.eng.2021.03.016

permeate flux of the membrane filtration system [5]. However, this aspect requires further investigation.

Microbial products and slowly biodegraded products [13,15,16] are the major components in the biofilm matrix [17]. Microorganisms play a key role in biofouling. Therefore, it is possible that biofouling can be alleviated by controlling the growth of microorganisms. Chlorine is commonly used worldwide in drinking water and wastewater treatment to inactivate pathogens and prevent waterborne diseases [18–21]. However, it remains unclear whether membrane fouling could be significantly alleviated by chlorinated water. Owing to the presence of fewer microorganisms, less membrane biofouling is expected. However, some microbial species are chlorine-resistant and the contribution of these bacteria to membrane fouling is still unknown. Furthermore, the hydrophobic/hydrophilic nature of the membrane is a critical parameter in the application and performance of membranes [22]. It influences the separation performance and selective permeability of the organics during membrane filtration [23]. Owing to the difference in the intercepted organics in their hydrophobicity/hydrophilicity, different bacterial communities can survive and result in the formation of different biofilms and consequently affect the filtration performance. However, relevant studies are limited despite its great significance.

Furthermore, Flemming and Wingender [24] reported that biofilms are aggregates of microorganisms. Cells are frequently embedded in a self-produced matrix of extracellular polymeric substances (EPS), indicating that investigation of the bacteria is also an indispensable requirement for the recognition and regulation of biofouling. Even in the same reverse-osmosis membrane water purification plant, the bacterial community differs among the various compartments, and membrane fouling is also different [25]. Wu et al. [26] also found differences in biofilm microorganisms when different filtration configurations were applied, although the feed water was the same. These studies indicate that the biofilm bacterial community is dynamic, complex, and needs to be considered as an essential aspect during the investigation of biofouling.

In this study, tap water (typical chlorinated water; low DOC ((2.920 ± 0.011) mg·L^{-1})) and lake water (a common surface water without any pretreatment; high DOC ((6.440 ± 0.039) mg·L^{-1})) were selected as the raw water from a practical standpoint, as they are representative of real-world water supplies. Thus, for people living in cities, public tap water commonly serves as drinking water prior to purification. However, for people living in remote areas, the available water source is commonly surface water, such as lake water. Additionally, two types of UF membranes, namely, polyvinylidene fluoride (PVDF) and polyether sulfone (PES) membranes, were compared in this study to investigate whether the hydrophobicity/hydrophilicity of the membrane affects the properties of the biofilm that forms. In addition, the properties of the biofilm, involving the morphology, functional groups, and matrix components, were investigated to elucidate the biofouling characteristics of these filtration systems. Special consideration was given to the bacterial community and diversity in the biofilms, and more importantly, to their biofouling mechanisms.

2. Materials and methods

2.1. Reactor construction and operation

Two types of water (tap water, after residual chlorine was removed, and lake water) were used in the study; tap water collected from the local water supply and lake water samples taken from the lake in the Olympic Park, Beijing, China. The source of the tap water was the Beijing No. 9 Water Treatment Plant. Before discharged from the water treatment plant, the water was disinfected by aqueous chlorination at a concentration of 1.2–1.8 mg·L^{-1} for 5 h. The concentration of the residual chlorine in the tap water was 0.07–0.08 mg·L^{-1}. After standing for at least 24 h (to allow the disappearance of chlorine), the tap water was used in the experiments. The water was collected every other day and stored in a 2 L container. The quality of the two types of water is given in Appendix A Table S1), where the tap water has a relatively low concentration of organic matter, whereas the lake water is composed of a wide range of organic substances. In addition, two types of UF membranes (Beijing Separate Equipment Co., Ltd., China) were employed for comparison: PVDF and PES. Each membrane had a filtration area of approximately 25 cm^2 and a molecular weight cutoff (MWCO) of 100 kDa, corresponding to 7–8 nm. Three GDM systems were operated in parallel, in dead end-mode, for 32 d at a constant pressure head of 40 mbar (1 bar = 10^5 Pa; Appendix A Fig. S1). These systems are denoted as tap water-PVDF, lake water-PVDF, and lake water-PES. In the course of filtration, permeate flux was recorded daily and calculated according to the method supplied in Appendix A Supplemental Materials and Methods. At the end of the operation, biofilms on the membrane in the three parallel filtration systems were taken out and prepared for analysis, as described in the following sections.

2.2. Molecular weight determination of the organics in the raw water, filtrate, and biofilm

High-performance size exclusion chromatography (HPSEC) was used to determine the molecular weight (MW) distribution of the organics. HPSEC was conducted with a binary high performance liquid chromatography (HPLC) pump (Waters 1525, USA) containing a BioSep-SEC-S3000 column (7.8 mm × 300 mm; Phenomenex, USA), a security guard column fixed with a GFC-3000 disc 4 mm inside diameter (ID), a series 200 pump, a photodiode array detector (Waters 2998, USA) operated at a wavelength of 254 nm, and an auto-sampler (Waters 2707, USA). A 10 mmol·L^{-1} sodium acetate solution (Sigma–Aldrich, USA) was used as the mobile phase at a flow rate of 1 mL·min^{-1}, and the injection volume per sample was 100 μL. Prior to measurement, the mobile phase was set at a flow rate of 2 mL·min^{-1} to purify the column. After the baseline was steady, the samples were run to acquire accurate results. The MW profiles were obtained according to the calibration data acquired using appropriate standard solutions. All samples were passed through a 0.22 μm filter prior to instrumental analysis.

To measure organics in the biofilm, approximately 0.25 cm^2 of each biofilm was cut and dissolved with 2 mL of 1% phosphate buffer solution in a 5 mL centrifuge tube. Before heating in a water bath at 80 °C for 20 min, the mixture was vortexed for approximately 2 h. Thereafter, 1.5 mL of the mixture was transferred to a new sterile 2 mL centrifuge tube and further centrifuged at 10 000 r·min^{-1} for 2 min. The supernatant was collected for subsequent measurements. Triplicate samples of the same area for each biofilm were selected for HPSEC measurements.

2.3. Fluorescent organics characterization in the raw water, filtrate, and biofilm

Excitation–emission matrix (EEM) fluorescence spectroscopy was performed with a Hitachi F-4600 fluorescence spectrophotometer (Japan) to investigate the presence of protein- or humic acid-like substances in the raw water, filtrate, and biofilm. The excitation (Ex) wavelength was in the range of 200–450 nm and the emission (Em) wavelength was between 250 and 550 nm, and the bandpass was 5 nm in both cases. To reduce interference from particles, water samples were filtered using a 0.45 μm needle filter before EEM analysis. Additionally, parallel factor (PARAFAC) analysis was conducted with MATLAB software.

2.4. Characterization of the hydrophilic and hydrophobic organics in the filtrate

The hydrophilic and hydrophobic organic substances in the filtrates were analyzed by separation using Superlite DAX-8 resins (Supelco, USA) and Amberlite XAD-4 (Rohm and Hass, USA) and fractionation into three groups: strongly hydrophobic substances (adsorbed by DAX-8), weakly hydrophobic (or transphilic) substances (adsorbed by XAD-4), and hydrophilic substances (permeating through both DAX-8 and XAD-4 resins). Prior to analysis, the resins were washed with methanol and deionized water several times to ensure that they were free of organic matter, as indicated by the DOC measurement. The pH of the sample water was adjusted to 2.0 prior to passing through the DAX-8 resin (at a rate of 5 mL·min^{-1}) and then the XAD-4 absorption column (at 15 mL·min^{-1}). According to the DOC values measured before and after the DAX-8 and XAD-4 resins, the concentrations of the three different components were determined. DOC values were determined using a total organic carbon analyzer (TOC-V, Shimadzu, Japan).

2.5. Determination of zeta potential and contact angle of the biofilm

The zeta potential of biofilms was measured using an electric solid surface analyzer (SurPASS 3, Anton Paar, Austria), and the contact angle of the biofilms was determined using a contact angle meter (Dataphysics, Germany). For the latter, five randomized locations were selected for the measurement, and the value was recorded continuously for more than 200 s.

2.6. Scanning electron microscopy (SEM) and atomic force microscopy (AFM) analysis of biofilm

Samples of biofilms and membranes were prepared for SEM (S-4800, Hitachi) analysis by freeze-drying and metal spraying on the surface. Thereafter, the images were taken off the surface and cross-section to reveal the three-dimensional (3D) morphology of the biofilms.

To elucidate the biofilm roughness and distribution patterns of the substances, AFM analysis was performed. Specifically, AFM micrographs of the three biofilms were obtained using a Bruker Dimension Icon ScanAsyst in PeakForce Tapping mode with a ScanAsyst Air tip (FASTSCANBIO, Bruker, Germany). Scans (10 μm × 10 μm) were acquired with a scan rate in the range of 0.1–0.3 Hz and a peak force setpoint between 8 and 15 nN. Trace and retrace scans were captured and inspected in the case of data uncertainty. Thereafter, each image was flattened and cleaned to remove scan defects using NanoScope Analysis software 1.8. In addition, particle analysis was performed using the same software, and fitting curves were plotted using Origin 2018 software (Electronic Arts Inc., USA).

2.7. Fourier transform infrared (FTIR) spectroscopy tests of the biofilms

To identify the specific functional groups in the biofilms, FTIR (Spectrum Two, PerkinElmer, USA) analysis was performed. In addition, FTIR mapping (Spotlight 400) was carried out to visually display the substances in the biofilms. The length and width of the biofilm samples were set at 500 μm in all cases (the three biofilms), and the spatial resolution was 6.25 μm × 6.25 μm. To reflect comprehensively the distribution of substances in the biofilms, at least three images were captured per biofilm.

2.8. Confocal laser scanning microscopy (CLSM) images of biofilm

Fresh biofilms with membranes were fixed with 2.5% formaldehyde immediately after removing from the filtration systems and then pasted onto glass coverslips using double-sided adhesive tape. Staining was performed in a dark environment with 10 μg·mL^{-1} fluorescein isothiocyanate (FITC, Sigma–Aldrich), which stains all proteins [27,28]; 10 μg·mL^{-1} Concanavalin A (ConA, Sigma–Aldrich), which binds α-mannopyranosyl and α-glucopyranosyl sugar residues [29]; and 10 μg·mL^{-1} 4′,6-diamidino-2-phenylindole (DAPI; Sigma–Aldrich), which stains extracellular DNA (eDNA) present within the biofilms [30]. Intermittent staining and rinsing were performed for each biofilm, with the staining procedure lasting 30 min, followed by rinsing with phosphate buffer; this was repeated several times. The presence of proteins, polysaccharides, and eDNA on the glass coverslips was visualized by CLSM (TCS SP5, Leica, Germany) [31–34]. Three channels were used with the corresponding Ex and Em wavelengths as follows: FITC (488 nm/520 nm), ConA (543 nm/560 nm), and DAPI (371 nm/397 nm). The *z*-stack confocal images obtained by CLSM were processed using ImageJ software (USA).

2.9. Molecular experiments and bioinformatics analysis

High-throughput sequencing technology was applied to provide detailed information regarding the bacterial community in the biofilms. 16S ribosome RNA (rRNA) V4 region was selected as the amplicon, which was considered to yield the greatest diversity at the domain and phylum levels [35]. DNA was extracted from the biofilms with an area of approximately 6.25 cm^2, using proteinase K and sodium dodecyl sulfate-based lysis [36], and purified with the DNA Clean and Concentrator-25 Kit (Zymo Research, USA) according to the manufacturer's protocol. Thereafter, the DNA quality was evaluated by ultraviolet (UV) spectrometry at wavelengths of 230, 260, and 280 nm (absorbance rates: 260 nm/280 nm, ~1.8; 260 nm/230 nm, > 1.8) detected using a NanoDrop-1000 spectrophotometer (NanoDrop Technologies, USA), and DNA integrity was assessed by 0.8% agarose gel electrophoresis. Ultimately, the whole DNA was stored at −20 °C until polymerase chain reaction (PCR) amplification.

The universal primers were used to amplify the 16S rRNA V4 region, containing forward primer 515F (5′-GTGCCAGCMGCCGCGGTAA-3′) and reverse primer 806R (5′-GGACTACHVGGGTWTCTAAT-3′) [35]. The barcodes were added to distinguish different samples, and Phusion® High-Fidelity PCR Master Mix with GC Buffer (New England Biolabs, USA) was used for amplification. After a series of reactions [37], PCR products were produced; hence, triplicate PCR products were combined and visualized using 1% agarose gel electrophoresis. In addition, the PCR products were purified with the GeneJET PCR Purification Kit (Thermo Scientific, USA), quantified using the Qubit dsDNA HS Assay Kit (Invitrogen, USA), and pooled at equal molality for subsequent sequencing. Sample libraries were prepared using the Ion Plus Fragment Library Kit 48 rxns (Ion Torrent, USA) and sequenced with an Ion S5™ XL sequencer (Thermo Scientific) using the single-end method at Novogene Bioinformatics Institute. Thereafter, the forward and reverse reads were joined and assigned to different samples based on barcodes. Primer sequences and barcodes at the end of each read were trimmed. Any joined sequences with ambiguous bases, length less than 100 bp or mean quality score small than 20, were discarded. In comparison with the reference data set (Greengenes database[†]) [38], chimeric sequences were removed from the clean sequences. Only effective sequences were used for further analysis. Hence, sequences were clustered into operational taxonomic units (OTUs) using the UPARSE pipeline [39] at a cutoff value of 97% nucleotide similarity, and taxonomic classification was performed with the representative sequences of each OTU using the Ribosomal Database Project classifier at a confidence threshold of 0.8 [40].

[†] http://greengenes.secondgenome.com.

Representative sequences were those with the highest frequencies. The Greengenes Database was adopted for taxonomic assignment, which has taxonomic categories anticipated to the species level. The sequence number in each sample was normalized to the same depth (70 301 sequences per sample) used in the subsequent comparative analysis. The raw sequencing reads were deposited in the National Center of Biotechnology Information (NCBI) Sequence Read Archive (SRA) database under accession number PRJNA692793.

Phylogenetic trees were constructed using the neighbor-joining (NJ) method in molecular evolutionary genetics analysis (MEGA) 6.0 [41], based on the representative sequence of each OTU, in which a Kimura two-parameter (K_2P) distance model was used to measure genetic divergences of OTUs, and thousand bootstrap trials were performed. Much information, such as the number of OTUs, reads per OTU, distribution of each taxon, and proportions of OTUs in each taxon, was supplemented using the interactive tree of life online tool [42]. Venn diagrams and circle graphs demonstrating species richness and abundance were drawn using R v3.5.2. Bar plots displaying the relative abundance of bacteria at the phylum level across different samples and biodiversity indices (e.g., Shannon index, Chao1 index, and ACE index) were completed in Origin 2018.

3. Results

3.1. Physico–chemical properties of biofilms in GDM systems

The initial permeate flux of the tap water-PVDF system was substantially greater than that of the other two systems (Fig. 1(a)). For the latter, the initial flux was very similar; however, it was slightly greater for the lake water-PES system. In all cases, the flux declined as a function of filtration time, although it gradually reached a near-stable condition on the 20th day, consistent with other findings observed under constant pressure [5,11]. However, under stable conditions, a slightly greater permeate flux was observed for the lake water-PVDF (1.23 $L{\cdot}m^{-2}{\cdot}h^{-1}$) and lake water-PES (1.24 $L{\cdot}m^{-2}{\cdot}h^{-1}$) systems than for the tap water-PVDF (1.10 $L{\cdot}m^{-2}{\cdot}h^{-1}$) system, in contrast to the corresponding values at the beginning of the operation. According to the results, the flux seemed unrelated to the hydrophobicity/hydrophilicity of the membrane; however, it may be influenced by the raw water, and the chlorinated water led to a lower flux than the surface water.

However, the accumulated biofilms were strongly hydrophobic, as illustrated by the contact angle (Fig. 1(b)), which was unrelated to the water treatment processes, suggesting the generality of the biofilm. In addition, it can be observed that the MW of the organics in all biofilms mainly ranged from 1 to 100 kDa (Fig. 1(c)), with a relatively higher value in the chlorinated-water biofilm (tap water-PVDF) than in the lake-water biofilms (lake water-PVDF and lake water-PES); therefore, more organics were present in the chlorinated-water biofilm. The stronger capacity of the microorganisms to secrete EPS in the chlorinated-water biofilm was the major reason for the greater accumulation of organics, as indicated by the same pore size of membranes and less organics in the tap water.

In addition, a less negative zeta potential was observed for the tap-water biofilm ((−24.50 ± 2.89) mV) than for the lake-water biofilms ((−29.83 ± 2.78) and (−29.27 ± 2.44) mV, respectively) (Fig. 1(d)), implying that it was easier (lower electrostatic repulsion) for substances to contact with, and be retained by, the biofilm in the tap-water system than the biofilms in the lake-water systems; this probably contributed to the greater amounts of organics

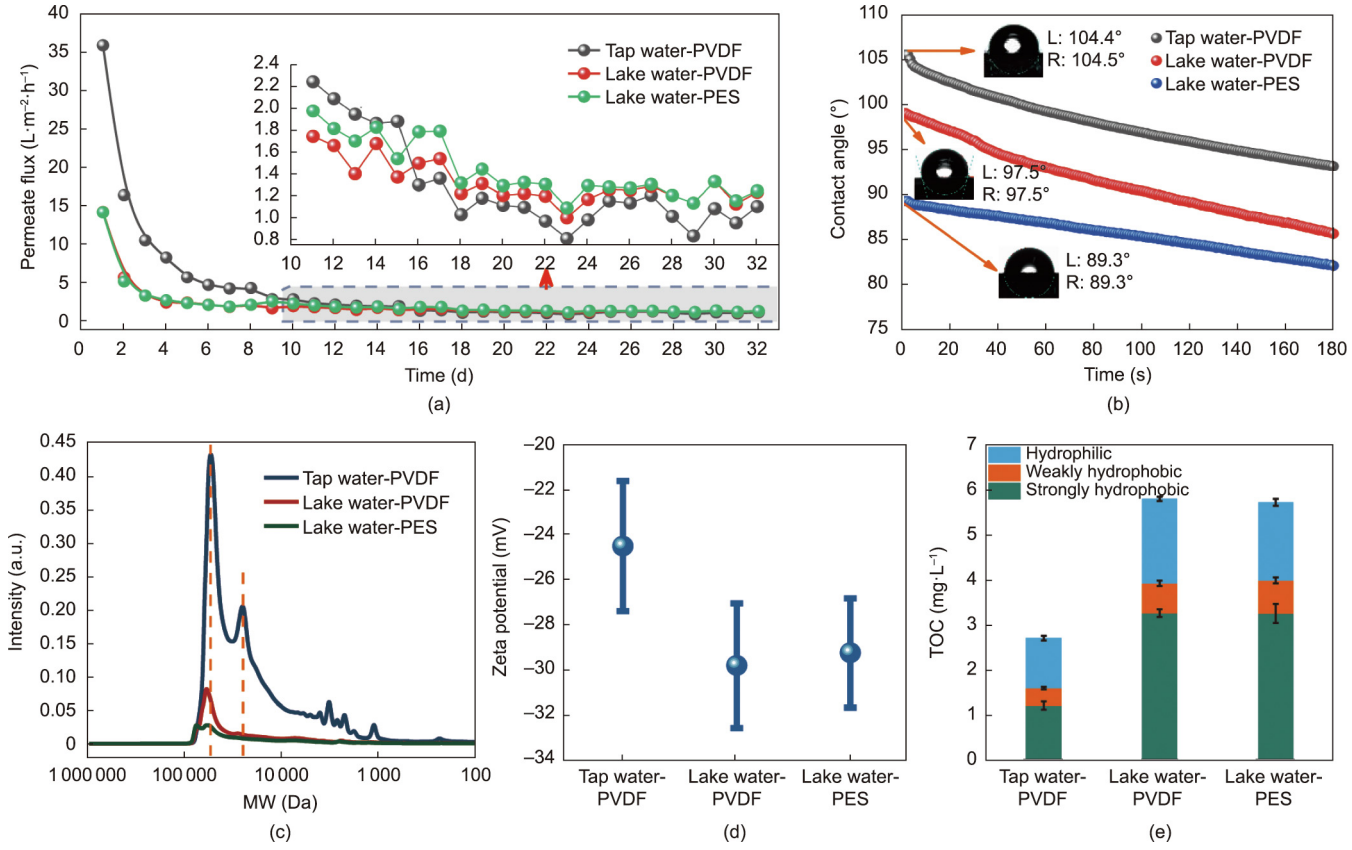

Fig. 1. Filtration performance and physico–chemical properties of the biofilms. (a) Variation of permeate flux during the period of operation (32 d). (b) The initial variation of contact angle of the biofilms with time (≤ 180 s). (c) MW distribution of organics in each biofilm treated with sodium hydroxide. (d) Surface zeta potential of each biofilm. (e) Hydrophilic/hydrophobic components of organics in the filtrates as indicated by the total organic carbon (TOC). Results shown in (b)–(e) are based on samples taken at the end of the experimental period.

in the former biofilm. For the lake-water biofilms formed on different membranes, the zeta potential values were close to each other. For the membrane filtrates, over 50% of the organics in all filtrates were strongly hydrophobic (Fig. 1(e)), whereas the proportion of the hydrophobic/hydrophilic substances displayed no substantial difference between the two lake-water systems, which also indicated the limited role of the hydrophilicity/hydrophobicity of the membrane, especially for long-term operating systems.

3.2. Morphological structure of the biofouling layer

The structure of the biofilm in the tap water-PVDF system appeared dense, with substances aggregated together and limited spaces between them (Fig. 2(a)). In contrast, the morphology of the lake-water biofilms, shown in Figs. 2(b) and (c), was markedly different from that of biofilms in the tap water-PVDF system, with a porous and "spider-web" structure formed. The biofilm accumulated in the tap water-PVDF system (12.8 μm) was thicker than the other two biofilms (5.8 μm for lake water-PVDF system; 8.8 μm for lake water-PES system; Figs. 2(d)–(f)). These observations provide strong and direct evidence for the effect of chlorinated water on membrane fouling, with more severe biofouling formed by tap water, suggesting that organics in the raw water might not be the only key factor for membrane fouling (lower value for tap water and higher value for lake water). In contrast, the bacteria retained by the membrane played an essential role, particularly chlorine-resistant species that were not removed by chlorine. Moreover, it was supposed that the bacteria intercepted by the membrane substantially affected the structure of the biofilm that was formed, as evidenced by the significant difference in biofilm morphology between the tap-water and lake-water filtration systems.

3.3. Particle and functional groups analysis of biofilm

Obtuse-shaped particles were observed in the tap-water biofilm, which was in contrast to the cuspidal-shaped particles in the lake-water biofilms, as shown by the 3D micrographs (Fig. 3). In addition, particle analysis demonstrated that a wider distribution of particles was present in the tap-water biofilm, ranging from 140 to 350 nm (frequency > 0.2) (Appendix A Fig. S2), while the corresponding range was 85–210 nm for the lake water-PVDF biofilm and 80–160 nm for the lake water-PES biofilm, respectively. Moreover, the biofilm roughness was greater for the tap water-PVDF biofilm ((71.7 ± 1.3) nm) than for the lake-water biofilms ((54.2 ± 1.2) nm for lake water-PVDF biofilm; (32.2 ± 0.9) nm for lake water-PES biofilm; Appendix A Table S2). These findings further revealed the size and morphology of substances in the biofilms and indicated the adverse effect of chlorine pretreatment on membrane fouling, as the particles were larger and more obtuse in the tap-water biofilm than those in the lake-water biofilms, which probably made it easier for them to induce more severe biofouling.

In functional groups, according to the images of FTIR mapping (Figs. 3(c), (g), and (k)) and corresponding spectra (Figs. 3(d), (h), and (l)), three main components were present in each biofilm, as displayed in different colors. Substance 1 was seen principally in the micrographs, followed by substances 2 and 3, as indicated by the frequency of different colors. Moreover, the spectrum of substance 1 in the lake water-PVDF and lake water-PES biofilms was similar, showing that analogous substances were retained or secreted by the microorganisms. The absorption bands of amide I (1640 cm^{-1}), amide II (1528 cm^{-1}), and amide III (1392 cm^{-1}) [43–47] were observed in all biofilms, suggesting a wide distribution of proteins, as these are characteristic peaks of proteins and essential components in forming proteins [46]. In addition, the presence of C–O at 1052 cm^{-1} signified the presence of polysaccharides in the biofilms [43].

Additionally, when comparing the spectra of the PVDF/PES membranes under contaminated (without biofilm) and clean conditions (Appendix A Fig. S3), significant variations are observed in several absorption bands. The contaminated PVDF membrane demonstrated intense absorption at 1651 cm^{-1} in all UF membranes, owing to the stretching vibration of amide I, suggesting that this protein appeared in the membrane. In the PES membrane, the absorption at O–H (stretching vibration) and $–CH_2–$ was markedly stronger in the clean than in the fouled ones (Appendix A Fig. S3(b)), indicating that the substances adhering to the membrane overlapped the location of absorption bands, and the presence of intercepted or excreted substances determined the type of functional groups.

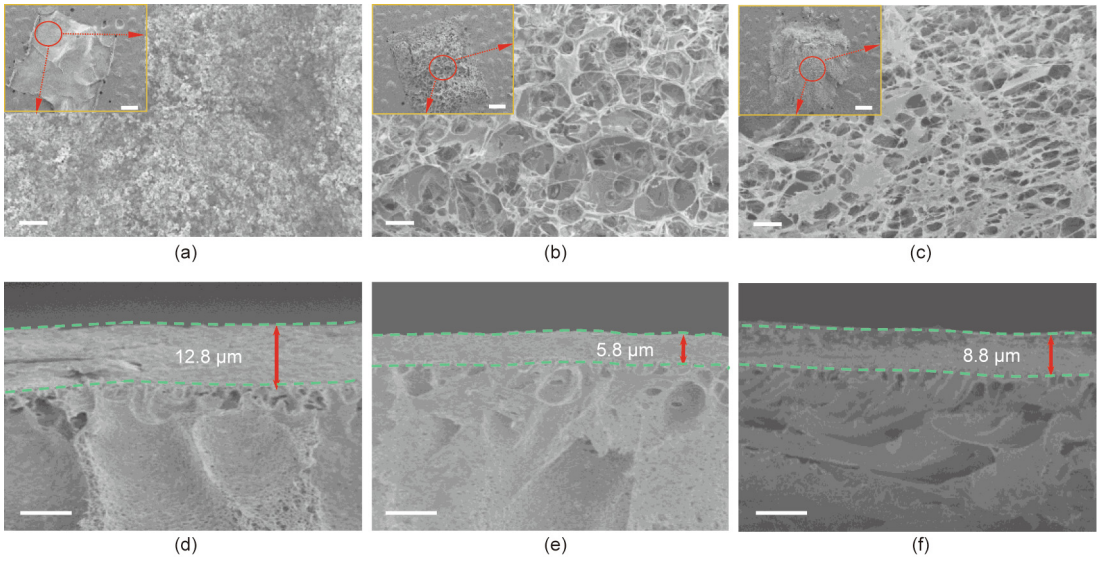

Fig. 2. SEM images of biofilms for the different gravity-driven filtration systems. (a–c) Surface micrographs of the three biofilms (tap water-PVDF, lake water-PVDF, and lake water-PES, respectively). The insets are initial pictures of each biofilm, and scale bars denote 500 μm. The outer photographs are the enlarged images of the red-boxed areas; scale bars denote 1, 100, and 100 μm from (a) to (c). (d)–(f) Images of the biofilms captured in cross-section (tap water-PVDF, lake water-PVDF, and lake water-PES, respectively); scale bars = 10 μm.

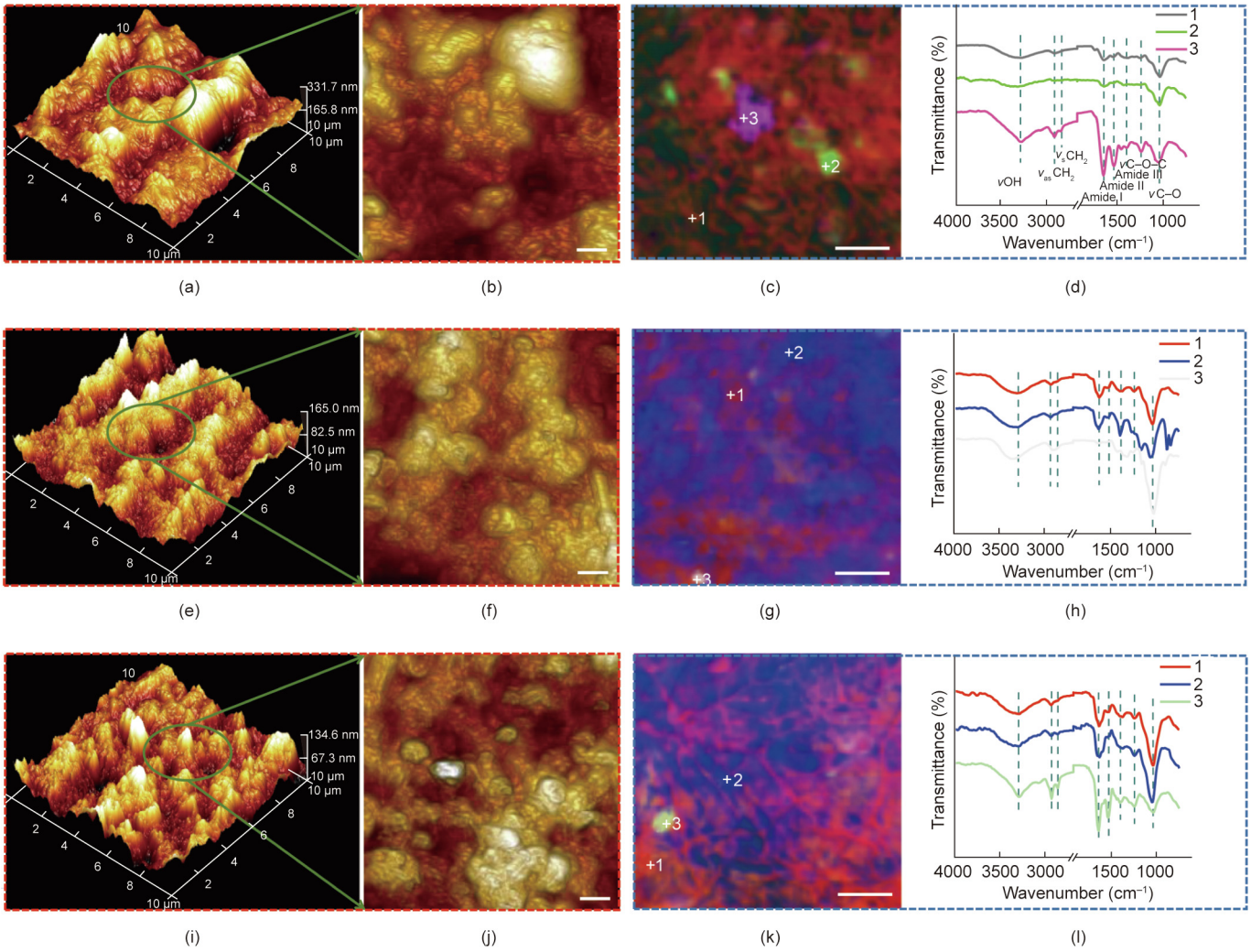

Fig. 3. *In-situ* AFM images and FTIR spectra of biofilms accumulated through filtration of tap water and lake water. Graphs in (a), (e), and (i) are 3D structures of each biofilm via AFM. (b), (f), and (j) refer to the surface morphology of the biofilms; scale bars = 1 μm. (c), (g), and (k) are *in-situ* infrared microscopy images of the three biofilms; scale bars = 100 μm. (d), (h), and (l) represent corresponding FTIR spectra of the cross marks in (c), (g), and (k). The top, middle, and bottom panels denote the samples of tap water-PVDF, lake water-PVDF, and lake water-PES, respectively. *v*: stretching vibration; as: asymmetrical; s: symmetrical.

3.4. Distribution patterns of biofilm matrix components

Polysaccharides (red) were more abundant in the three biofilms than proteins (green) and eDNA (blue; Figs. 4(a)–(c), Appendix A Movies S1–S3), as indicated by the fluorescence intensity of each color. A multitude of polysaccharides and eDNA were present in the dense biofilm of the tap water-PVDF system, and their magnitudes were relatively larger than those in the other two biofilms. In contrast, relatively few proteins were evident, presumably because of the type of bacterial species present (lower protein excretion). The biofilms accumulated in the lake-water systems had a loose structure, as discussed previously. Combined with the SEM results,

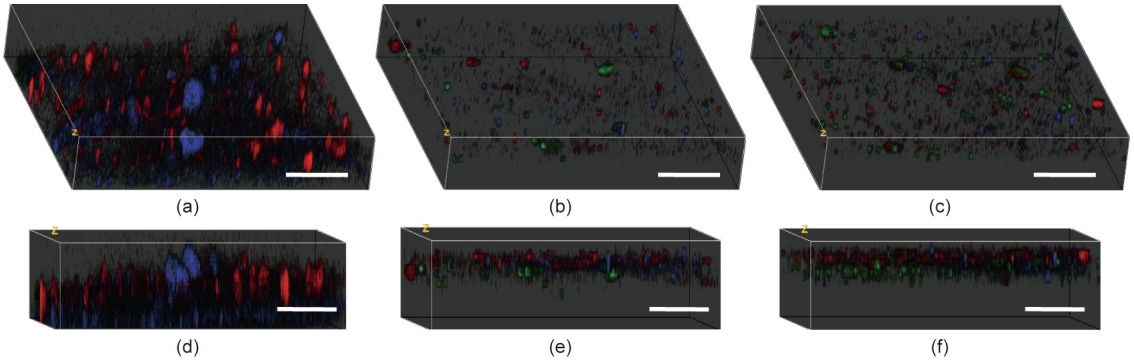

Fig. 4. Confocal laser scanning micrographs of the biofilms stained with FITC for proteins (green), ConA for polysaccharides (red), and DAPI for eDNA (blue). (a)–(c) The images of each biofilm are captured from the top aspect (tap water-PVDF, lake water-PVDF, and lake water-PES, respectively). (d)–(f) Distribution patterns of the three components are elucidated from the front view for each biofilm. Each picture is the stacked synthesis of a series of micrographs obtained by scanning the biofilm in the *z*-axis. Representative of 10 recorded locations. Scale bars = 50 μm.

it was clear that the thick tap-water biofilm was largely owing to the presence of polysaccharides, which was a vitally important influencer on membrane filtration performance. Furthermore, we found that proteins were mainly located at the bottom of the biofilms, whereas polysaccharides and eDNA were principally seen in the upper part of the biofilm layer (Figs. 4(d)–(f)). The spatial determination of these components made it clear that it was the protein that was connected directly to the surface of the membrane, and this was consistent with the results of FTIR analysis of the membrane.

3.5. Dissection of bacterial community in biofilm

According to the phylogenetic tree based on the sequences of OTUs (Fig. 5(a)), approximately 20 taxa were obtained from high-throughput sequencing data at the phylum level in samples of the three biofilms. It was evident that the number of OTUs belonging to Proteobacteria was the largest, followed by Bacteroidetes and Planctomycetes. In terms of relative abundance (Fig. 5(b)), a simple bar plot showed that Proteobacteria, Bacteroidetes, and Planctomycetes occupied a principal position in the three biofilms. Proteobacteria accounted for a proportion greater than 50%, suggesting their significance in biofilms. Specifically, the proportions of Proteobacteria and Bacteroidetes were strikingly higher in the tap-water biofilm than in the lake-water biofilms. In contrast, the bacterial community was similar for the two lake-water biofilms at the phylum level, as evidenced by the similar relative abundance of Proteobacteria (48.54% and 48.19% for lake water-PVDF and lake water-PES, respectively), Bacteroidetes (8.90% and 8.06%), Planctomycetes (25.87% and 30.26%), Actinobacteria (5.15% and 4.76%), and Chlamydiae (3.18% and 3.12%). Moreover, according to the Venn diagram (Fig. 5(c)), a total of 251 OTUs were present in all three biofilms, and an overlap of 641 OTUs was observed in the two lake-water biofilms, which also confirmed the limited influence of membrane hydrophobicity/hydrophilicity on biofilm bacterial community. Detailed information associated with the species of three phyla Proteobacteria, Bacteroidetes, and Planctomycetes in richness and abundance is provided in Figs. S4 and S5 and Supplemental Materials and Methods in Appendix A.

Based on previous research, the 20 most abundant genera associated with OTUs and reads were examined for smaller taxa (genus). In OTUs (Fig. 6(a)), one essential indicator of richness, *Gemmata*, *Planctomyces*, and *Prosthecobacter* accounted for the highest value in all biofilms, whereas *Rhodoplanes*, *Rhodobacter*, and *Pseudomonas* were among the least diverse. In addition, variability was found in the different biofilms for the same genus. For instance, *Aquicella* occupied higher OTUs in lake-water biofilms; however, it was lower in the tap-water biofilm.

As shown in Fig. 6(b), which represents the abundance of species, the number varied from 1 (e.g., *Kaistia* and *Polynucleobacter* (tap water-PVDF)) to 20 133 (*Xanthobacter* (tap water-PVDF)). *Xanthobacter* can produce copious amounts of slime [48], which is also referred to as EPS. Therefore, the formation of a thick biofouling layer in the tap water filtration system is clearly deciphered. In addition, members of *Xanthobacter* can utilize halogenated alkanes as their sole carbon source and conduct dehalogenation with chlorinated aliphatic and chloroaromatic compounds [48]. Thus, it can be justified that *Xanthobacter* occupies a dominant position in the bacterial community. Regarding lake-water biofilms, a consistent variation was observed for the mentioned genera. This could be due to the accumulation of biofilm on the surface of the membrane as a function of time, which adversely influenced the selectivity of the membrane. Furthermore, as illustrated by the Shannon index [49], Chao1 index [50], and ACE index [51] (Appendix A Fig. S6), the bacterial community was less diverse in the tap-water biofilm than in the lake-water biofilms.

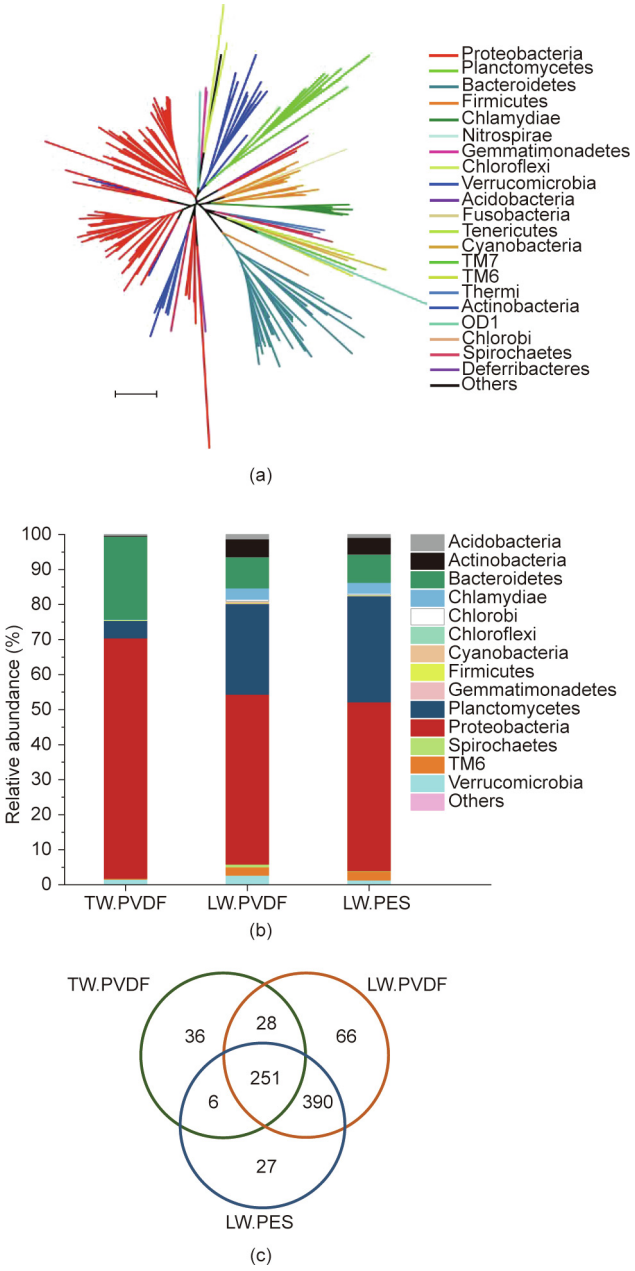

Fig. 5. Phylogenetic trees based on the sequencing data and relative abundance of bacteria across the three biofilms of the different filtration systems. (a) Tree diagram of presentative sequences in all taxonomies. Distance was measured as the number of base substitutions based on the K_2P method. Scale bar represents 0.1. (b) Relative abundance of bacteria across different biofilms at the phylum level. (c) Venn diagram of OTUs shared in the three biofilms. TW.PVDF refers to tap water-PVDF, LW.PVDF means lake water-PVDF, and LW.PES denotes lake water-PES.

3.6. Removal performance of organics in the filtration system

To further investigate the differences in the biofilms and their role in the filtration system, the removal performance of organics was studied. As demonstrated by EEM fluorescence spectroscopy, there were mainly two peaks ($\lambda_{Ex}/\lambda_{Em}$ = 220–250 nm/280–330 nm and $\lambda_{Ex}/\lambda_{Em}$ = 250–290 nm/280–330 nm) observed in the raw and filtered waters (Figs. 7(a)–(c)). These were attributed to tyrosine-like substances, according to the conventional EEM "peak picking" technology [52]. When comparing the fluorescence spectra in the same filtration system, it was clear that the intensity of tyrosine-like substances was substantially reduced by the membranes and

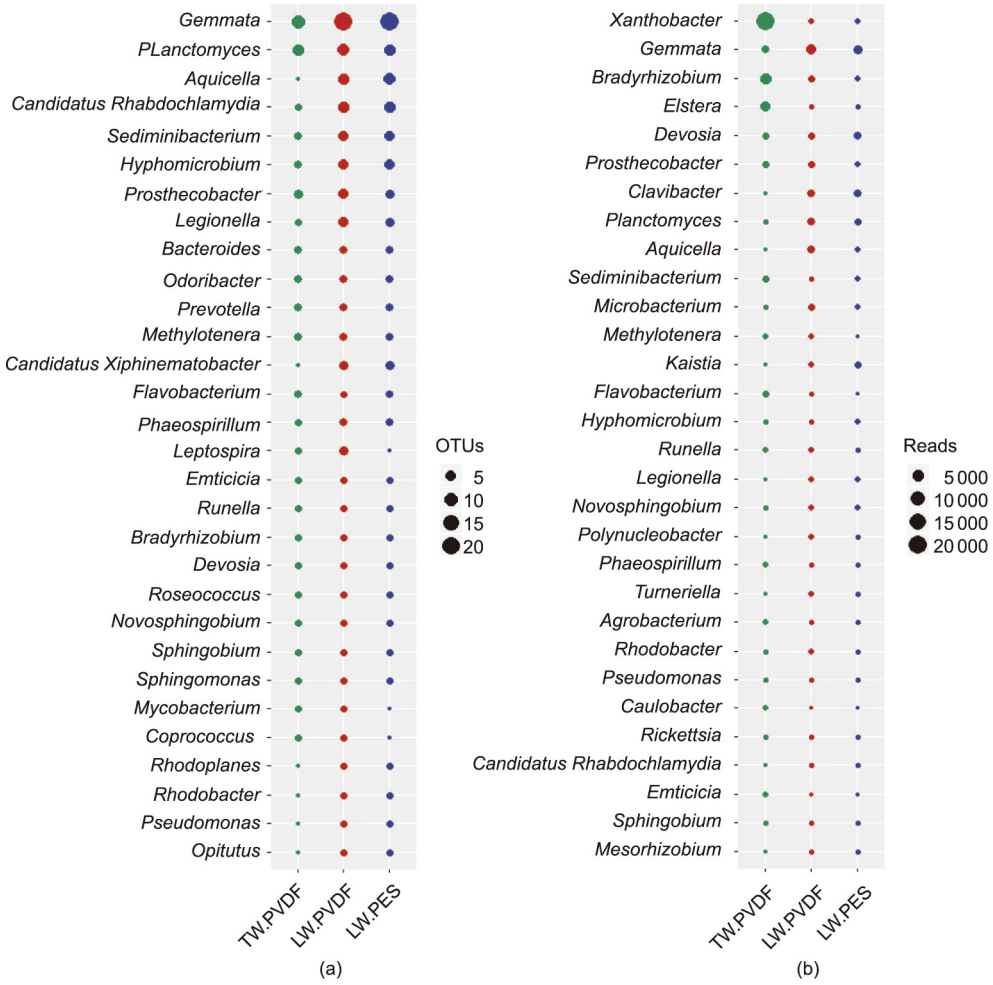

Fig. 6. (a) Richness and (b) abundance of the top 20 genera in different biofilms, where the size of the circle represents the value of each parameter and different colors denote different biofilms.

attached biofilms, regardless of the type of feed water and membrane.

Furthermore, the fluorescence signal of the organics was decomposed into underlying individual fluorescent phenomena by PARAFAC analysis [53,54] to quantify and trace the variations of different organic fractions [55], which were chemically independent but spectrally overlapping. The results revealed that the fluorescence substances could not be further decomposed for the raw and filtered waters in the tap water-PVDF system, suggesting that tyrosine-like substances were independent and not spectrally affected by other components. In contrast, in all the samples of both lake-water systems, the organics were decomposed into three components comprising tyrosine-, fulvic acid-, and humic-like substances (Appendix A Figs. S7 and S8), by searching with the OpenFluor database[†], which contained a large library of published PARAFAC results. It was clear that the species of fluorescent substances in the water were not changed by the filtration system, although the fluorescence intensity varied. Thus, a decrease was apparent for tyrosine-like substances in the filtered waters when compared with those in the influent waters, whereas the intensity barely changed for the other two components, indicating that the fluorescent matter removed was tyrosine-like substances. Furthermore, as measured by HPSEC (Figs. 7(d)–(f)), the MW of the removed organics was in the range of 20–100 kDa for all filtration systems, which corresponded well to the presence of "biopolymers" [56–58] and verified the key role of bacteria in the formation of such organics.

4. Discussion

In this study, the effects of commonly used water (chlorinated water and lake water) on membrane fouling, the roles of membrane hydrophobicity/hydrophilicity during biofouling formation, and the related key microorganisms were investigated. This involved extended bench-scale tests using GDM UF technology and analysis of the morphology, physicochemical properties, matrix (EPS), and bacterial community of biofilms. It was found that significantly different biofilms were formed by tap water and lake water. Moreover, a greater degree of membrane fouling was observed for the tap-water filtration system than the lake-water system, as evidenced by the lower value of permeate flux and greater thickness of biofilm. In a previous study [5], the concentration of DOC was shown to have an essential influence on the level of permeate flux stabilization, with a greater value of DOC positively correlated with lower flux. However, in this study, a contrary result was found, implying that other important factors (e.g., bacteria) might be involved in addition to DOC.

The tap-water biofilm presented a densely compact morphology and was consistent with other findings achieved through the addition of sodium azide, which suppressed biological activity

[†] https://openfluor.lablicate.com/.

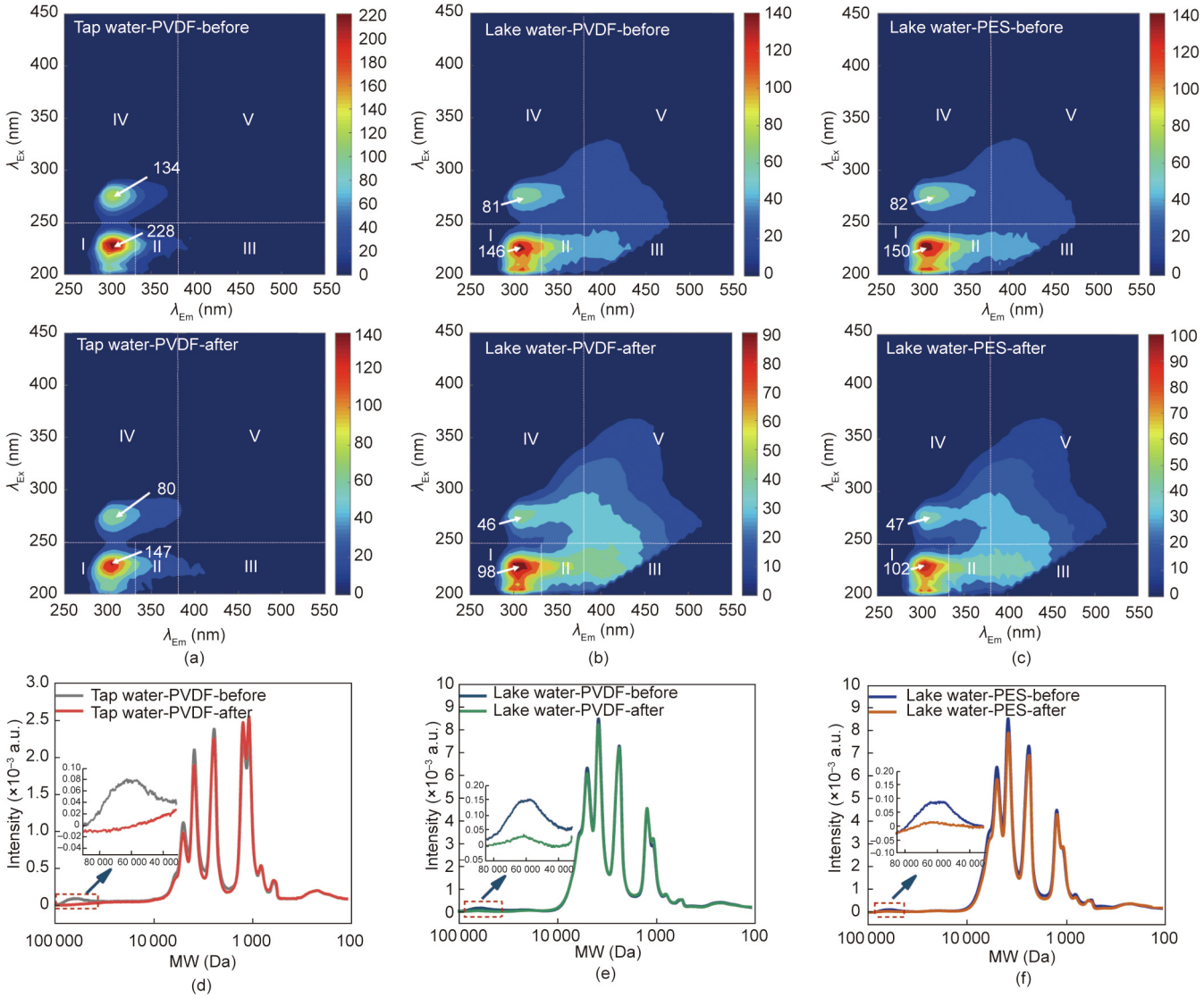

Fig. 7. Nature of organic matter in influent water and filtrate for the different filtration systems (tap water-PVDF, lake water-PVDF, and lake water-PES): (a)–(c) EEM fluorescence spectra, and (d)–(f) MW distributions. The regions I–V represent tyrosine-, tryptophan-, fulvic acid-, soluble microbial by-product-, and humic acid-like substances, respectively. All analyses were performed at the end of the experimental period. The suffixes "-before" and "-after" represent the influent water and filtrate, respectively.

[5], indicating that while a majority of bacteria were killed, the remaining bacteria plausibly excreted more EPS, leading to an even more compact structure and severe membrane fouling. In contrast, a porous, spider web-like structure of the biofilm was formed in the lake-water systems. The significantly different behavior can be explained by the following two reasons. First, each microorganism has its certain EPS, exerting dissimilar membrane fouling. A different bacterial community is assumed to induce a dissimilar structure of biofilm. Akhondi et al. [11] showed that the presence of different microorganisms had a significant effect on biofouling morphology. Bae et al. [59] also highlighted the crucial role of bacteria in biofilm formation. Second, EPS distribution patterns altered the structure of the biofilm. Although the major components were proteins, polysaccharides, and eDNAs, as confirmed by FTIR tests, the different distribution patterns of these components may lead to a distinct morphology of the biofilm. As illustrated by CLSM in this investigation, the shape and size of the major components were significantly different between tap-water and lake-water biofilms, resulting in a different structure of the biofouling layer. Desmond et al. [15] also proposed that the EPS composition was linked to the biofilm physical structure, showing that lower concentrations of polysaccharides and eDNA coincided with greater heterogeneity in the physical structure of the biofilm, which was also demonstrated by SEM results in this study.

Polysaccharides and eDNAs were principally located in the upper part of the biofilm layer as shown by CLSM, whereas proteins were chiefly observed at the bottom, which were unrelated to the type of influent water and membrane employed. It is believed that this is the first study to provide spatial information on the three main EPS components, which can help understand the functions they perform within the biofilm layer. Polysaccharides and eDNAs provide shelter for bacteria to withstand adverse external factors. As for proteins, owing to the abundant functional groups, they can bind tightly with the active layer of the membrane, thereby facilitating bacterial growth on the surface of the membrane and securing biofilm formation.

When exploring the biofilm bacterial community, it can be observed that *Xanthobacter* was the dominant taxon in the tap-water biofilm, which could produce copious amounts of slimes (EPS) [48]. Moreover, members of *Xanthobacter* have been reported

to feed on haloalkanes and halocarboxylic acids [60,61]. They could produce haloalkane dehalogenase to release chloride from halogenated chemicals [61]. Accordingly, the extremely high abundance of *Xanthobacter* in the tap-water biofilm was not difficult to understand. Moreover, these bacteria, which were not removed by chlorine, could generate powerful forces in biofouling and are of major significance. However, previous research has not provided sufficient information on *Xanthobacter* in tap water, because of limitations related to the source of tap water (surface or underground water), the employed sequencing technology (Illumina [62] or 454 pyrosequencing technology [63]), and the smallest taxon (phylum [63], family [64], or genus [65]). Furthermore, owing to the limited number of sequenced samples in this study, the experimental group comparisons were not used for statistical analysis. However, according to the results of the bacterial composition analysis, key taxa in the different biofilms were obtained.

Membrane hydrophobicity/hydrophilicity played a minor role in influencing the biofouling properties, as verified by the results of SEM images, zeta potential, functional groups, and CLSM images. This is because of the accumulated biofilm that overlaid the active layer of the membrane, thereby reducing its significance. Moreover, as the biofilm matured, its properties were progressively determined by the influent water.

In summary, this experimental investigation revealed the effect of chlorinated water on membrane fouling and the resulting biofouling properties and exposed some of the bacteria-driven mechanisms of biofilm accumulation. We believe that this study provides a greater understanding of the key role of chlorine-resistant bacteria in biofouling formation from an ecological perspective and will contribute substantially to future improvements in the control of membrane fouling.

5. Conclusions

In this study, we found greater membrane fouling during the filtration of chlorinated water (tap water) than untreated surface water (lake water), as indicated by the lower permeate flux and greater thickness of the biofilm. A densely compact morphology was observed for the tap-water biofilm; in contrast, a porous, spider-like structure was found in the lake-water biofilms, which was closely related to the microbial community. Based on the 16S rRNA sequencing results, *Xanthobacter* was the dominant taxon in the tap-water biofilm. In addition, a larger quantity of polysaccharide and eDNA was present in the tap-water biofilm than in the lake-water biofilms, suggesting the key role of polysaccharides and eDNA in membrane fouling. However, membrane hydrophobicity/hydrophilicity played only a minor role in affecting the membrane fouling properties and microbial community. Moreover, to our knowledge, this study is the first to discover the commonness in distribution patterns of the major matrix components in the vertical direction, with proteins located mainly in the lower parts of biofilms, and polysaccharides and eDNA principally found in the upper parts, which has important implications for understanding the roles they play in biofilm maintenance.

Acknowledgments

This research was financially supported by the Key Research and Development Plan of the Ministry of Science and Technology, China (2019YFD1100104 and 2019YFC1906501).

Compliance with ethics guidelines

Li Zhang, Lei Xu, Nigel Graham, and Wenzheng Yu declare that they have no conflict of interest or financial conflicts to disclose.

Appendix A. Supplementary data

Supplementary data to this article can be found online at https://doi.org/10.1016/j.eng.2021.03.016.

References

[1] Mekonnen MM, Hoekstra AY. Four billion people facing severe water scarcity. Sci Adv 2016;2(2):e1500323.
[2] Desmond P, Morgenroth E, Derlon N. Physical structure determines compression of membrane biofilms during gravity driven membrane (GDM) ultrafiltration. Water Res 2018;143:539–49.
[3] Chawla C, Zwijnenburg A, Kemperman AJB, Nijmeijer K. Fouling in gravity driven point-of-use drinking water treatment systems. Chem Eng J 2017;319:89–97.
[4] Gao W, Liang H, Ma J, Han M, Chen ZL, Han ZS, et al. Membrane fouling control in ultrafiltration technology for drinking water production: a review. Desalination 2011;272(1–3):1–8.
[5] Peter-Varbanets M, Hammes F, Vital M, Pronk W. Stabilization of flux during dead-end ultra-low pressure ultrafiltration. Water Res 2010;44(12):3607–16.
[6] Peter-Varbanets M, Margot J, Traber J, Pronk W. Mechanisms of membrane fouling during ultra low pressure ultrafiltration. J Membr Sci 2011;377(1–2):42–53.
[7] Ding An, Wang J, Lin D, Tang X, Cheng X, Li G, et al. *In situ* coagulation versus pre-coagulation for gravity-driven membrane bioreactor during decentralized sewage treatment: permeability stabilization, fouling layer formation and biological activity. Water Res 2017;126:197–207.
[8] Ding An, Liang H, Li G, Szivak I, Traber J, Pronk W. A low energy gravity-driven membrane bioreactor system for grey water treatment: permeability and removal performance of organics. J Membr Sci 2017;542:408–17.
[9] Wang Y, Fortunato L, Jeong S, Leiknes T. Gravity-driven membrane system for secondary wastewater effluent treatment: filtration performance and fouling characterization. Sep Purif Technol 2017;184:26–33.
[10] Ding A, Wang J, Lin D, Cheng X, Wang H, Bai L, et al. Effect of PAC particle layer on the performance of gravity-driven membrane filtration (GDM) system during rainwater treatment. Environ Sci Water Res Technol 2018;4:48–57.
[11] Akhondi E, Wu B, Sun S, Marxer B, Lim W, Gu J, et al. Gravity-driven membrane filtration as pretreatment for seawater reverse osmosis: linking biofouling layer morphology with flux stabilization. Water Res 2015;70:158–73.
[12] Derlon N, Mimoso J, Klein T, Koetzsch S, Morgenroth E. Presence of biofilms on ultrafiltration membrane surfaces increases the quality of permeate produced during ultra-low pressure gravity-driven membrane filtration. Water Res 2014;60:164–73.
[13] Ding An, Liang H, Li G, Derlon N, Szivak I, Morgenroth E, et al. Impact of aeration shear stress on permeate flux and fouling layer properties in a low pressure membrane bioreactor for the treatment of grey water. J Membr Sci 2016;510:382–90.
[14] Klein T, Zihlmann D, Derlon N, Isaacson C, Szivak I, Weissbrodt DG, et al. Biological control of biofilms on membranes by metazoans. Water Res 2016;88:20–9.
[15] Desmond P, Best JP, Morgenroth E, Derlon N. Linking composition of extracellular polymeric substances (EPS) to the physical structure and hydraulic resistance of membrane biofilms. Water Res 2018;132:211–21.
[16] Chomiak A, Traber J, Morgenroth E, Derlon N. Biofilm increases permeate quality by organic carbon degradation in low pressure ultrafiltration. Water Res 2015;85:512–20.
[17] Pronk W, Ding An, Morgenroth E, Derlon N, Desmond P, Burkhardt M, et al. Gravity-driven membrane filtration for water and wastewater treatment: a review. Water Res 2019;149:553–65.
[18] Park KY, Choi SY, Lee S-H, Kweon JH, Song JH. Comparison of formation of disinfection by-products by chlorination and ozonation of wastewater effluents and their toxicity to *Daphnia magna*. Environ Pollut 2016;215:314–21.
[19] Li Z, Liu X, Huang Z, Hu S, Wang J, Qian Z, et al. Occurrence and ecological risk assessment of disinfection byproducts from chlorination of wastewater effluents in East China. Water Res 2019;157:247–57.
[20] Deborde M, von Gunten U. Reactions of chlorine with inorganic and organic compounds during water treatment-kinetics and mechanisms: a critical review. Water Res 2008;42(1–2):13–51.
[21] Diana M, Felipe-Sotelo M, Bond T. Disinfection byproducts potentially responsible for the association between chlorinated drinking water and bladder cancer: a review. Water Res 2019;162:492–504.
[22] Knozowska K, Kujawski W, Zatorska P, Kujawa J. Pervaporative efficiency of organic solvents separation employing hydrophilic and hydrophobic commercial polymeric membranes. J Membr Sci 2018;564:444–55.
[23] Zhao L, Wu C, Lu X, Ng D, Truong YB, Zhang J, et al. Theoretical guidance for fabricating higher flux hydrophobic/hydrophilic dual-layer membranes for direct contact membrane distillation. J Membr Sci 2020;596:117608.
[24] Flemming HC, Wingender J. The biofilm matrix. Nat Rev Microbiol 2010;8(9):623–33.
[25] Bereschenko LA, Heilig GH, Nederlof MM, van Loosdrecht MC, Stams AJ, Euverink GJ. Molecular characterization of the bacterial communities in the

different compartments of a full-scale reverse-osmosis water purification plant. Appl Environ Microbiol 2008;74(17):5297–304.
[26] Wu B, Suwarno SR, Tan HS, Kim LH, Hochstrasser F, Chong TH, et al. Gravity-driven microfiltration pretreatment for reverse osmosis (RO) seawater desalination: microbial community characterization and RO performance. Desalination 2017;418:1–8.
[27] Akram KM, Yates LL, Mongey R, Rothery S, Gaboriau DCA, Sanderson J, et al. Live imaging of alveologenesis in precision-cut lung slices reveals dynamic epithelial cell behaviour. Nat Commun 2019;10(1):1178.
[28] Teirlinck E, Xiong R, Brans T, Forier K, Fraire J, Van Acker H, et al. Laser-induced vapour nanobubbles improve drug diffusion and efficiency in bacterial biofilms. Nat Commun 2018;9(1):4518.
[29] Yu W, Xu L, Graham N, Qu J. Pre-treatment for ultrafiltration: effect of pre-chlorination on membrane fouling. Sci Rep 2014;4(1):6513.
[30] Denis K, Le Bris M, Le Guennec L, Barnier JP, Faure C, Gouge A, et al. Targeting Type IV pili as an antivirulence strategy against invasive meningococcal disease. Nat Microbiol 2019;4(6):972–84.
[31] Kuijl C, Savage NDL, Marsman M, Tuin AW, Janssen L, Egan DA, et al. Intracellular bacterial growth is controlled by a kinase network around PKB/AKT1. Nature 2007;450(7170):725–30.
[32] Lawrence JR, Neu TR. Confocal laser scanning microscopy for analysis of microbial biofilms. Methods Enzymol 1999;310:131–44.
[33] Schlafer S, Meyer RL. Confocal microscopy imaging of the biofilm matrix. J Microbiol Methods 2017;138:50–9.
[34] Castello M, Tortarolo G, Buttafava M, Deguchi T, Villa F, Koho S, et al. A robust and versatile platform for image scanning microscopy enabling super-resolution FLIM. Nat Methods 2019;16(2):175–8.
[35] Peiffer JA, Spor A, Koren O, Jin Z, Tringe SG, Dangl JL, et al. Diversity and heritability of the maize rhizosphere microbiome under field conditions. Proc Natl Acad Sci USA 2013;110(16):6548–53.
[36] Yuan J, Li M, Lin S, Hoheisel JD. An improved DNA extraction method for efficient and quantitative recovery of phytoplankton diversity in natural assemblages. PLoS ONE 2015;10(7):e0133060.
[37] Guo X, Zhou X, Hale L, Yuan M, Ning D, Feng J, et al. Climate warming accelerates temporal scaling of grassland soil microbial biodiversity. Nat Ecol Evol 2019;3(4):612–9.
[38] DeSantis TZ, Hugenholtz P, Larsen N, Rojas M, Brodie EL, Keller K, et al. Greengenes, a chimera-checked 16S rRNA gene database and workbench compatible with ARB. Appl Environ Microbiol 2006;72(7):5069–72.
[39] Edgar RC. UPARSE: highly accurate OTU sequences from microbial amplicon reads. Nat Methods 2013;10(10):996–8.
[40] Wang Q, Garrity GM, Tiedje JM, Cole JR. Naive Bayesian classifier for rapid assignment of rRNA sequences into the new bacterial taxonomy. Appl Environ Microbiol 2007;73(16):5261–7.
[41] Tamura K, Stecher G, Peterson D, Filipski A, Kumar S. MEGA6: molecular evolutionary genetics analysis version 6.0. Mol Biol Evol 2013;30(12):2725–9.
[42] Letunic I, Bork P. Interactive tree of life (iTOL) v3: an online tool for the display and annotation of phylogenetic and other trees. Nucleic Acids Res 2016;44(W1):W242–5.
[43] Schmitt J, Flemming HC. FTIR-spectroscopy in microbial and material analysis. Int Biodeter Biodegr 1998;41(1):1–11.
[44] Sailakshmi G, Mitra T, Sinha S, Chatterjee S, Gnanamani A, Mandal AB. Suberic acid acts as a dissolving agent as well as a crosslinker for natural polymers (carbohydrate and protein): a detailed discussion on the chemistry behind the interaction. J Macromol Sci Part A Pure Appl Chem 2012;49(8):619–29.
[45] Mann D, Teuber C, Tennigkeit SA, Schröter G, Gerwert K, Kötting C. Mechanism of the intrinsic arginine finger in heterotrimeric G proteins. Proc Natl Acad Sci USA 2016;113(50):E8041–50.
[46] Jung H, Pena-Francesch A, Saadat A, Sebastian A, Kim DH, Hamilton RF, et al. Molecular tandem repeat strategy for elucidating mechanical properties of high-strength proteins. Proc Natl Acad Sci USA 2016;113(23):6478–83.
[47] Edington SC, Gonzalez A, Middendorf TR, Halling DB, Aldrich RW, Baiz CR. Coordination to lanthanide ions distorts binding site conformation in calmodulin. Proc Natl Acad Sci USA 2018;115(14):E3126–34.
[48] Wiegel J. The genus *Xanthobacter*. In: Dworkin M, Falkow S, Rosenberg E, Schleifer KH, Stackebrandt E, editors. The prokaryotes. Volume 5: Proteobacteria: alpha and beta subclasses. New York: Springer; 2006. p. 290–314.
[49] Hill MO. Diversity and evenness: a unifying notation and its consequences. Ecology 1973;54(2):427–32.
[50] Causey BD. Parametric estimation of the number of classes in a population. J Appl Stat 2002;29(6):925–34.
[51] Chao A, Lee SM. Estimating the number of classes via sample coverage. J Am Stat Assoc 1992;87(417):210–7.
[52] Chen W, Westerhoff P, Leenheer JA, Booksh K. Fluorescence excitation—emission matrix regional integration to quantify spectra for dissolved organic matter. Environ Sci Technol 2003;37(24):5701–10.
[53] Stedmon CA, Bro R. Characterizing dissolved organic matter fluorescence with parallel factor analysis: a tutorial. Limnol Oceanogr Methods 2008;6(11):572–9.
[54] Bahram M, Bro R, Stedmon C, Afkhami A. Handling of Rayleigh and Raman scatter for PARAFAC modeling of fluorescence data using interpolation. J Chemometr 2006;20(3-4):99–105.
[55] Wünsch UJ, Murphy KR, Stedmon CA. The one-sample PARAFAC approach reveals molecular size distributions of fluorescent components in dissolved organic matter. Environ Sci Technol 2017;51(20):11900–8.
[56] Yu W, Liu T, Crawshaw J, Liu T, Graham N. Ultrafiltration and nanofiltration membrane fouling by natural organic matter: mechanisms and mitigation by pre-ozonation and pH. Water Res 2018;139:353–62.
[57] Yu W, Graham NJD, Fowler GD. Coagulation and oxidation for controlling ultrafiltration membrane fouling in drinking water treatment: application of ozone at low dose in submerged membrane tank. Water Res 2016;95:1–10.
[58] Yu W, Zhang D, Graham NJD. Membrane fouling by extracellular polymeric substances after ozone pre-treatment: variation of nano-particles size. Water Res 2017;120:146–55.
[59] Bae H, Kim H, Jeong S, Lee S. Changes in the relative abundance of biofilm-forming bacteria by conventional sand-filtration and microfiltration as pretreatments for seawater reverse osmosis desalination. Desalination 2011;273(2–3):258–66.
[60] Abe Y, Zopfi J, Hunkeler D. Effect of molecule size on carbon isotope fractionation during biodegradation of chlorinated alkanes by *Xanthobacter autotrophicus* GJ10. Isotopes Environ Health Stud 2009;45(1):18–26.
[61] Rozeboom HJ, Kingma J, Janssen DB, Dijkstra BW. Crystallization of haloalkane dehalogenase from *Xanthobacter autotrophicus* Gj10. J Mol Biol 1988;200(3):611–2.
[62] Ling F, Whitaker R, LeChevallier MW, Liu WT. Drinking water microbiome assembly induced by water stagnation. ISME J 2018;12(6):1520–31.
[63] Lin W, Yu Z, Zhang H, Thompson IP. Diversity and dynamics of microbial communities at each step of treatment plant for potable water generation. Water Res 2014;52:218–30.
[64] Li C, Ling F, Zhang M, Liu WT, Li Y, Liu W. Characterization of bacterial community dynamics in a full-scale drinking water treatment plant. J Environ Sci 2017;51:21–30.
[65] Liu G, Ling FQ, van der Mark EJ, Zhang XD, Knezev A, Verberk JQJC, et al. Comparison of particle-associated bacteria from a drinking water treatment plant and distribution reservoirs with different water sources. Sci Rep 2016;6(1):20367.